Proceedings of the ASME 2024
International Mechanical Engineering Congress and Exposition
IMECE2024
November 17-21, 2024, Portland, OR

IMECE2024-144955

POTENTIAL SAFETY HAZARDS ASSOCIATED WITH LI-ION BATTERY THERMAL RUNAWAY VENT GAS HEAT TRANSFER IN ENERGY STORAGE SYSTEMS

Ala' E. Qatramez[1], Andrew Kurzawski[2], John Hewson[2], Michael Meehan[2], Daniel Foti[1], Alexander J. Headley[1,*]

[1]Department of Mechanical Engineering, University of Memphis, Memphis, Tennessee, 38152
[2]Fire Science and Technology Department, Sandia National Laboratories, Albuquerque, New Mexico, 87185

ABSTRACT

This study focuses on assessing the safety hazards associated with Lithium-ion batteries vent gas in energy storage systems due to convective heating. Heat fluxes and convection heat transfer coefficients of vent gas at the module top surface are estimated. This analysis was carried out by CFD and thermal runaway model simulations. Four cases of two gap heights between the cells and walls of their module (H) and two vent gas jet velocities (v_{Jet}) are investigated. v_{Jet} values used in the simulations were based on venting predictions for failing 5 Ah and 10 Ah cells, and the two gap heights are selected based on estimates from a deployed system. The simulations results show that the vent gas could play a vital role in module-to-module thermal runaway propagation by pre-heating the cells in adjacent modules. Multiple sequential failures are needed to initiate a thermal runaway in the cell directly exposed to the vent gas jet. The analysis shows that the vent gas jet temperature has a significant effect on the number of failures needed to raise the exposed cell surface temperature to a dangerous level.

Keywords: Li-ion batteries, Vent gas, Thermal runaway

1. INTRODUCTION

Lithium-ion (Li-ion) batteries have been increasingly utilized in energy storage systems (ESSs) due to their high energy density and many other special specifications [1, 2]. Along with these special characteristics, Li-ion cells show thermal instability under extreme physical conditions, overheating, overcharging [3–5] or simply due to defects in the cell. Such abnormal situations, exothermic reactions between cell materials can lead to thermal runaway, where significant heat is released associated with a sharp increase in cell temperature. During thermal runaway, the failing cell ejects high temperature and combustible gases [6, 7] which can be hazardous to the safety of the rest of the system.

To understand the mechanics of thermal runaway, numerous works investigated single cell failures for different cell types, capacities, and chemistry [8–10]. However, beyond single cell failure, a large-scale safety issue in ESSs is the propagation of thermal runaway from a failing cell to other cells and modules in the ESS, where the hazards can increase significantly. Thermal runaway propagation cases were reported [11–13]. Such events resulted in significant financial losses and serious injuries [11].

Among the heat transfer pathways that drive thermal runaway, conduction has been widely investigated and mitigation methods have been suggested [14–18]. Despite all of these efforts, convective propagation by vent gas [19], and the associated potential safety hazards still need more investigation. In addition to the explosive nature of vent gases, convective propagation represents another potential hazard due to their high vent temperature. During venting, these gases spread in the module gap as shown in Fig. 1 and transfer heat to the top module surface, and the cells in the same module. Cells in adjacent modules can also be heated by the gases through the module case as shown in Fig. 1 even if no combustion occurs. Such effect is called, in this work, the local range effect, where only cells in direct interaction with the jet are affected. When the gases leave the module, many possible scenarios could happen including, but not limited to, additional spreading in the ESS and heat transfer to other modules and parts within the system (such as combustible plastics), or they could explode if the gas mixture is within the flammability limit. These scenarios can pose a rack-scale fire and explosion hazard. Such cases as well as the local range effects can be related to module-to-module propagation.

This work focuses on addressing and assessing the potential safety hazards associated with the local effects of the vent gas due to convection based on two venting speeds associated with two cell capacities, and two gap heights between the cells and walls of their module selected based on estimates from a deployed system. To achieve that, simulations will be used to emulate the vent gas jet in the gap between cells and the module walls where the vent gas stream is modeled as an impinging jet ejected out of the cell. Heat fluxes and convection heat transfer coefficients

*Corresponding author: jheadley@memphis.edu

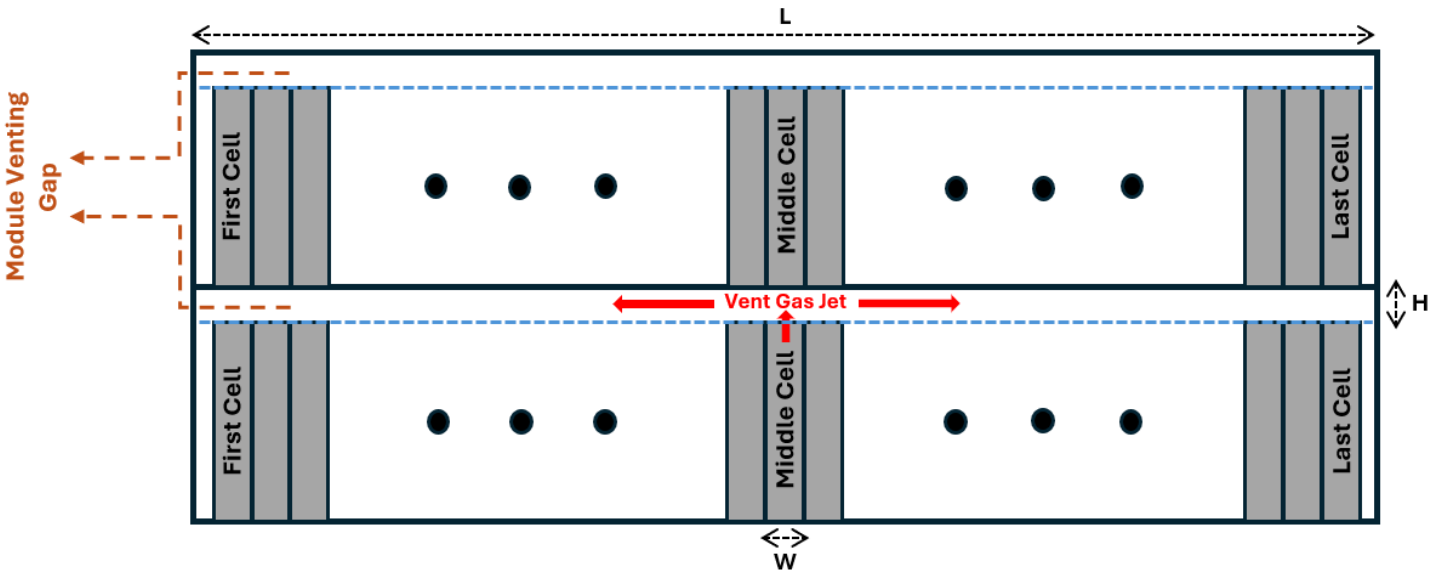

FIGURE 1: Front view of a simple schematic of two batteries' modules showing vent gas ejecting from the middle cell, movement of the vent gas in the module gap, cell thickness (W), gap height (H), and length (L). This figure is not to scale.

along the gap between the cells and their module walls will be estimated. The velocity and temperature evolution along the channel will be tracked. Finally, the 1D thermal runaway model, Lithium-ion Modeling with 1-D Thermal Runaway (LIM1TR), will be used to evaluate the potential for thermal initiation due to this hot vent gas jet. By that, insights on the role of vent gas in module-to-module thermal runaway propagation will be provided and evaluated which is the main goal of this work which can widen our understanding of such thermal events and help in designing batteries modules and safety vent openings. This paper is organized as follows, section 2 summarizes the model used to investigate the heat fluxes from the vent gas, computational field, and grid. The results will be discussed in section 3, and conclusions will be drawn in section 4.

2. METHODOLOGY

In this section, the solver, RANS model, LIM1TR, and the four cases were introduced and discussed. The velocity and temperature conditions, as well as the simulated domains were presented.

2.1 Simulations

The heat transfer solver, buoyantPimpleFoam, from the open-source package OpenFoam was used to simulate the vent gas impinging jet [20, 21]. The numerical solution is for two-dimensional transient and compressible continuity, Navier-Stokes, and energy equations for a flow of fixed vent gas mixture of volume fractions of 30% CO_2, 30% CO, 30% H_2, and 10% C_2H_4. These fractions are a round approximation from [6]. This solver is suitable to simulate different heat transfer and ventilation flows [20]. The turbulence is modeled with k-w Shear-Stress Transport RANS model [22, 23]. No reactions between gas species in the simulations.

The governing equations of the solver are presented as in Refs. [24, 25], where the conservation of mass is:

$$\frac{\partial \rho}{\partial t} + \nabla \cdot (\rho \mathbf{U}) = 0, \tag{1}$$

where $\mathbf{U}$ is the velocity field. The conservation of momentum:

$$\frac{\partial (\rho \mathbf{U})}{\partial t} + \nabla \cdot (\rho \mathbf{U}\mathbf{U}) - \nabla \cdot (\rho \nu_{eff} D(\mathbf{U})) = -\nabla p + \rho \mathbf{g}\,, \tag{2}$$

where $D(\mathbf{U}) = \nabla \mathbf{U} + (\nabla \mathbf{U})^T - \frac{2}{3}(\nabla \cdot \mathbf{U})\mathbf{I}$. ν_{eff} is the effective viscosity and $\mathbf{g}$ is the gravitational acceleration field. The conservation of energy:

$$\begin{aligned} \frac{\partial (\rho h)}{\partial t} + \nabla \cdot (\rho \mathbf{U} h) + \frac{\partial (\rho K)}{\partial t} + \nabla \cdot (\rho \mathbf{U} K) \\ - \frac{\partial p}{\partial t} = \nabla \cdot (\alpha_{eff} \nabla h) + \rho (\mathbf{g} \cdot \mathbf{U}), \end{aligned} \tag{3}$$

where α_{eff} is the effective thermal diffusivity and K is the kinetic energy per unit mass.

This work is based on 2D simulations of the module venting gap shown in Fig. 2 since the vent is approximated as a slot jet by assuming a pouch cell tears along the entire long edge and vents upward. 3D simulations can be used to capture the effect of the geometry of an actual tear. The module gap dimension is ($L \times H$), where L and H are the venting channel length and height, respectively. Two domains are simulated with ($1\ m \times 0.01\ m$), and ($1\ m \times 0.02\ m$), where the gap size, H, changes to study the effects of the length of H on the results as it will be shown. The grid is stretched in the streamwise and transverse directions with uniform distribution in the streamwise direction along the tear width (W). The grid cells (N) are 120000 for both domains with $Nx = 800$ and $Ny = 150$ grid cells in the streamwise and transverse direction, respectively.

Figure 2 shows the temperature of the inflow gas jet $T_{Jet} = 800\ ^\circ C$ which was used as vent gas temperature at the thermal

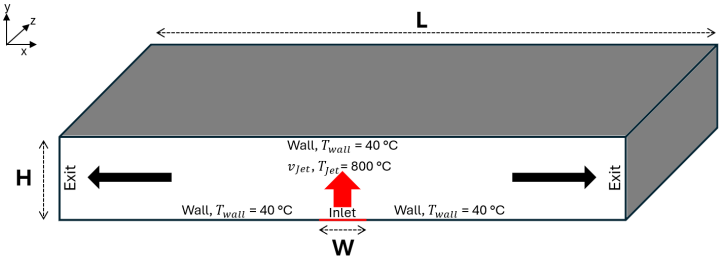

FIGURE 2: Representation of the simulated 2D domain of the module's gap. The boundary conditions: inlet, walls, and exits are shown. Gap dimensions (height (H) and gap length (L)), and tear width (W) are pointed out. The fixed values of the vent gas jet temperature (T_{Jet}) and wall temperatures (T_{wall}) are presented. The jet exits with a velocity of v_{Jet}. This figure is not to scale.

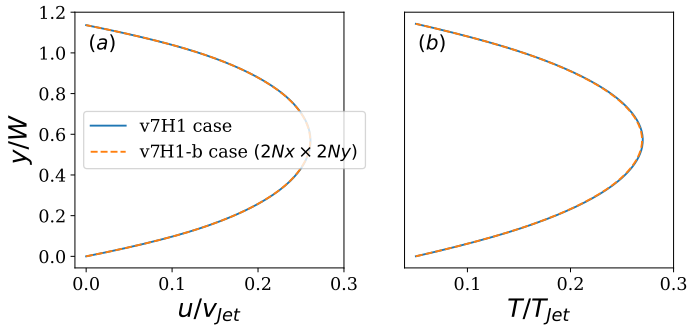

FIGURE 3: (a) normalized streamwise velocity (u/v_{Jet}) and (b) normalized temperature (T/T_{Jet}) profiles at x = 0.95 m for the v7H1 and v7H1-b cases.

runaway. The initial temperature and velocity in channel are $T_{initial}$ = 25°C and $U_{initial}$ = 0 m/s, respectively. Figure 2 also shows the boundary conditions of fixed wall temperature of T_{wall} = 40 ^{o}C that was imposed to represent the operating temperature of Li-ion cells. A turbulence intensity of 0.02 is used [26] to calculate the inlet turbulent kinetic energy of the gas jet.

In this effort, four thermal runaway cases are simulated with two venting velocities (v_{Jet}), and two channel heights. These cases are summarized in Table 1. v_{Jet} values are calculated based on two pouch cells with different capacities from [27] assuming full tear along the cell top surface. W also changes since the tear width is assumed to be the cell width. The simulation results were verified with a DNS simulation in Ref. [28].

2.2 Heat Flux

One of the main goals is to estimate the local heat fluxes (q'') and convection heat transfer coefficients (h) of these gases on the cell subjected to them. The heat flux at the top wall which the cells in contact with (see Fig. 1 and Fig. 2) were calculated as

$$q'' = -k\left(\frac{dT}{dy}\right)_{wall}, \tag{4}$$

where k and $(dT/dy)_{wall}$ are the thermal conductivity of the vent gas mixture and temperature gradient in the direction perpendicular to the wall, respectively. k is calculated at T_{wall}. Convection heat transfer coefficients, h, were calculated from Newton's law of cooling as

$$h = \frac{q''}{(T_{Jet} - T_{wall})} \tag{5}$$

2.3 LIM1TR

Scenarios of preheating of cells in an adjacent module by the vent jet are modeled in LIM1TR by employing the finite volume method and time integration from Spitfire to solve quasi-1D heat equations, chemical source terms are not modeled as this study is concerned with the heat transfer from convection up to the point of thermal runaway in the adjacent module [29–31]. Several boundary condition options can be applied to emulate different thermal runaway scenarios.

LIM1TR will be used to test the potential thermal runaway initiation by the cell vent gas. This will be done by applying convective boundary conditions informed by the CFD simulations on the surface of the corresponding cell to the vent gas jet.

3. RESULTS AND DISCUSSION

We aim to assess and quantify the thermal safety hazards associated with the vent gases in ESSs for all cases, where the effects of v_{Jet} and H are investigated. To do that, the flow field evolution in the module venting channel is studied, then the heat fluxes and convection heat transfer coefficients are calculated. After that, we evaluate by using LIM1TR the possibility of initiating thermal runaway by these gases; each of these will be discussed in detail below.

3.1 Mesh Independence Study

A sensitivity study of the grid was performed for v7H1 case to ensure that the results are mesh-independent. Figure 3 shows the profiles of streamwise velocity (u) normalized by v_{Jet} and temperature (T) over T_{Jet} at x = 0.95 m in module gap for v7H1 case, and v7H1-b case with the number of grid cells of 480000 ($2Nx \times 2Ny$) which is four times the cells number of v7H1 case. Both velocity and temperature profiles from Fig. 3 show that the results are independent on the number of the grid cells used to create the domain.

3.2 Flow Field

The profiles of the streamwise velocity and temperature are tracked at three x locations along the channel for all cases to form a view of u and T evolution, especially their values at the end of the channel which gives an idea about the thermal and kinetic energies that these gases have when they leave the channel.

Figure 4 shows the streamwise velocity and temperature profiles at x = 0.65, 0.75, and 0.95 m for all cases after the flow reached steady state. Figure 4(a) and (b) show u and T profiles for cases v7H1 and v7H2, respectively, while u and T profiles for case v5H1 and case v5H2 are shown in Fig. 4(c) and (d), respectively. The effects of H and v_{Jet} on u and T is clear. We can see from comparing Fig. 4(a) and (b) (v7H1 and v7H2) the effect of changing H on u, where u values along the channel noticeably decrease as H is doubled, and the same trend is shown in Fig. 4(c)

TABLE 1: The simulated cases of the four different thermal runaway scenarios with their corresponding cell capacities and dimensions.

Case	V_{Jet} (m/s)	H (cm)	Capacity (Ah)	Dimensions (mm)
Case 1: v7H1	7	1	5	67.4×62.1×8.8
Case 2: v7H2	7	2	5	67.4×62.1×8.8
Case 3: v5H1	5	1	10	150.4×57.8×10.4
Case 4: v5H2	5	2	10	150.4×57.8×10.4

and (d) for case v5H1 and case v5H2. For all cases, u decreases moving along the channel as the profiles show for the three x locations in the figure.

Temperature profiles for all cases show the same trend as the velocity, where T decreases along the channel as shown in Fig. 4. By comparing case v7H1 with case v7H2, and case v5H1 with case v5H2, gas temperature shows lower values for cases with smaller H moving away from impinging point which is opposite to the trend of u. Also, higher temperature values at $x = 0.95$ m are associated with the higher jet velocity ($v_{Jet} = 7$ m/s) for the same H.

Temperature and velocity profiles in Fig. 4 show that these gases leave the module in an ESS with high temperature ($T > 198$ °C) and relatively high velocity ($u \approx 0.85$ to 1.8 m/s) as the profiles at $x = 0.95$ m show. This represents potential safety hazards by the vent gas outside the module at a rack scale where they can spread in a rack and transfer heat to other cells, modules, and parts in that rack or ESS.

3.3 Local Heat Flux And Convection Heat Transfer Coefficients Estimations

The local heat fluxes and convection heat transfer coefficients for the four cases are discussed highlighting the influence of v_{Jet} and H on their magnitude and distribution along the channel, and extending the understanding of this influence on the safety hazards and module geometry design. The estimated heat fluxes and convection coefficients are shown in Fig. 5.

First, we can see that case v7H1 (the biggest v_{Jet} and smallest H) is associated with the highest values of q'' and h at the impingement point, where case v5H2 (the smallest v_{Jet} and biggest H) is associated with the lowest values of q'' and h at that point. From this, we can suggest that designing modules with relatively large gap heights reduces the potential hazards related to direct impinging heating from failing cell to corresponding cells in the above module, where the maximum heat flux q''_{max} decreases by about 21% and 25.2% by doubling H (from 1 cm to 2 cm) for cases v7H1 and v5H1 , respectively. v7H2, v5H1, and v5H2 cases have a smoother drop compared with v7H1, where a second peak appears just before 10 cm from the impingement point. After about 20 cm from the impingement, q'' and h profiles for all cases come closer to each other as the gas approaches channel flow.

Considering v7H1 case as the reference case, we can see that q''_{max} decreases more in case v7H2 than case v5H1 as shown in Fig. 5, and that is because H changes by 100% from 1 cm (in case v7H1) to 2 cm (in case v7H2), while v_{Jet} decreased by about 28.5% from 7 m/s (in case v7H1) to 5 m/s (in case v5H1). From that, it can be suggested to design cells with large vent opening

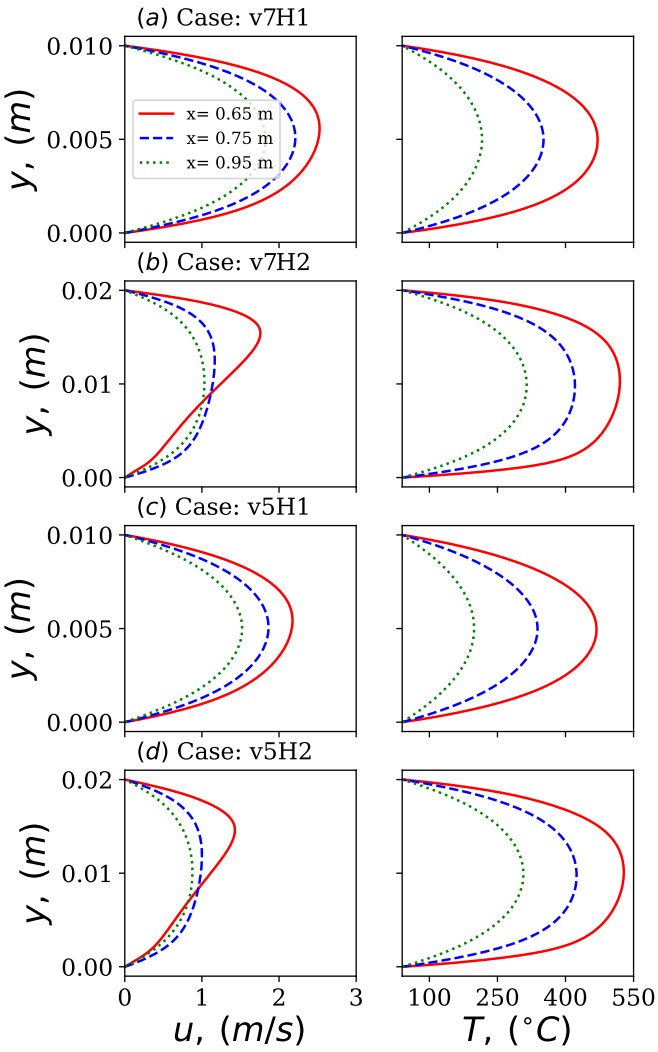

FIGURE 4: Streamwise velocity (u), and temperature (T) profiles at different locations along the channel: $x = 0.65, 0.75$, and 0.95 m for (a) v7H1 case, (b) v7H2 case, (c) v5H1 case, and (d) v5H2 case.

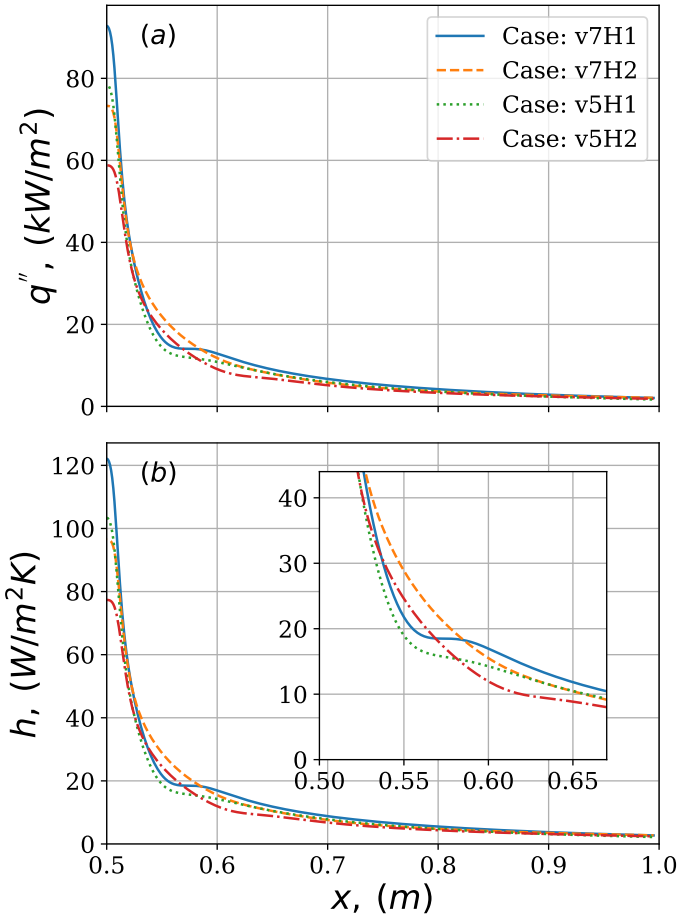

FIGURE 5: (a) local heat fluxes (q'') and (b) local convection heat transfer coefficients (h) for all cases.

to force the gases to exit with relatively low venting velocity to decrease the heat fluxes from direct impinging applied on the module wall. It is worth mentioning that though decreasing venting velocity decreases q''_{max} on the module wall, it also increases the residence time these gases take staying in the module gap since the residence time is associated with the mass flux in the channel which is related to v_{Jet}. This suggests further investigation on the effect of increasing residence time on thermal hazards compared with decreasing direct q''_{max}. Increasing the module gap height, H, has also the same effect on q''_{max} and residence time, where increasing H decrease q''_{max} and increases the residence time.

Table 2 shows q''_{max} and the percent of change in q''_{max} with respect to case v7H1 (q''_{max}%) due to increasing H and decreasing v_{jet}. This table shows the effect of v_{Jet} and H on q''_{max}, such quantitative presentation shows the sensitivity of q''_{max} to these parameters which provides insights on battery module design.

3.4 Potential Thermal Runaway Initiation

In this section, LIM1TR was used to test the amount of pre-heating and the possibility of a thermal runaway induced by the vent gas jet. A convective boundary condition of h estimated from the CFD simulations and T_{Jet} is applied on the cell surface

TABLE 2: The maximum heat flux (q''_{max}) for all cases and the percent of the change (%) in q''_{max}, H, and v_{Jet} with respect to case v7H1.

Case	q''_{max} (kW/m^2)	V_{Jet}%	H%	(q''_{max}%)
v7H1	92.8	-	-	-
v7H2	73.3	0%	+ 100%	- 21%
v5H1	78.6	- 28.5%	0%	- 15.3%
v5H2	58.8	- 28.5%	+ 100%	- 36.6%

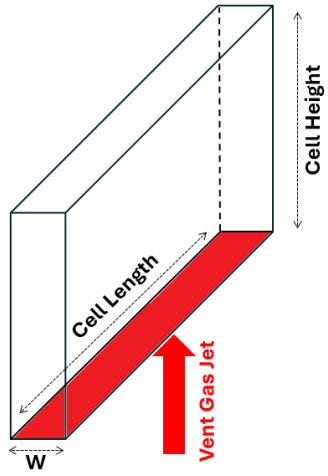

FIGURE 6: LIM1TR domain showing the cell dimensions. The red arrow represents the vent gas jet and the red face is where the jet is applied. This figure is not to scale.

exposed to the vent gas jet as shown in Fig. 6. The cell under interest here is the middle cell in the top module in Fig. 1.

3.4.1 Direct Repeated Heating. The estimated maximum convection coefficients (h_{max}) for case v7H1 (122.1 W/m^{2}K) and case v5H2 (77.4 W/m^{2}K) were used as boundary conditions on cell surface (see Fig. 6) with two values of T_{Jet} of 800 and 500 ° C. v7H1 and v5H2 cases are used as the two limits of the four cases in Table 2.

The goal, here, is to estimate the number of cell failures needed to initiate thermal runaway in the cell exposed to the jet ($n_{cell,TR}$) assuming that the thermal runaway occurs when the cell surface temperature (T_{cell}) is 200 °C according to the temperature measurements in Ref. [32] for single-cell experiments. While investigating the number of needed cells to failure, we also account for ($n_{cell,100}$) and ($n_{cell,150}$) which are the number of cell failures needed to heat the exposed surface of the middle cell to 100 and 150 °C, respectively, which helps in understanding the effect of the vent gas on module-to-module propagation as increased pre-heating can increase propagation speed [33]. Emphasizing that using a constant h_{max} as convective boundary condition represents an upper bound to examine extreme scenarios.

The venting times (t_{vent}) used are 11 and 14 s for 5 Ah and 10 Ah cells [32], respectively. The time between two vents ($t_{pre-heating}$) is 4 and 8 s for 5 Ah and 10 Ah cells [32], respectively. It is worth mentioning that the thicknesses of the cells, W,

in this work are different than those for cells in Ref. [32], since the thicknesses affects the propagation time across the cell width. LIM1TR simulations results are summarized in Table 3.

The results in Table 3 provides three main aspects related to vent gas convective hazards: 1) the sensitivity to h or h_{max} and T_{Jet} in terms of the number of cell failures to reach the three chosen temperatures, 2) the potential that these gases have to initiate thermal runaway in the exposed cell, this cell is the middle cell in the top module in Fig. 1, and 3) the significance of pre-heating in module-to-module propagation.

Regarding the sensitivity to h_{max} and T_{Jet}, LIM1TR simulations results show that the number of sequential cell failures needed to rise the middle cell surface temperature to the chosen temperatures is more sensitive to T_{Jet} than h_{max}, since the 36.6% decrease in h_{max} has a maximum increase in the number of required failures by 66.7%, while the 37.5% decrease in T_{Jet} has a minimum decrease of 90.9% in the number of required failures. The temperature of vent gas depends on many variables and it is not a design parameter. However, h or h_{max} is related to design parameters such as H and here suggestions can be provided to designing modules with relatively higher gap sizes to reduce the hazards due to direct impinging heating represented by h_{max}.

Considering the potential that vent gas has to initiate thermal runaway in the exposed cell, LIM1TR simulations results from the four simulated scenarios in Table 3 show that it requires at least 13 sequential cell failures assuming that the thermal runaway temperature is 200 °C. Such number of cell failures may refer to a possibility of thermal runaway initiation by pure convection considering these simulated conditions of direct impinging heating with constant h_{max}. These results lead to consideration of how convection by vent gas affects module-to-module propagation.

With this assumed condition of direct heating to bottom cell side, LIM1TR results show that vent gases play a role in pre-heating the cells in the upper module rather than driving them directly into thermal runaway where the first scenario in Table 3 shows, for example, that 3 consecutive cell failures can raise T_{cell} to 100 °C. In these scenarios, where there is no combustion involved, the vent gas plays a role in accelerating the thermal runaway in the adjacent module by pre-heating. This may have a vital role in module-to-module propagation where the pre-heating by vent gas is one of several major avenues of heat transfer including conduction through structural materials, deposition of solid ejecta, or the presence of external flames.

Figure 7(a) shows the evolution of the cell surface temperature and average cell temperature ($T_{average}$) over time for Scenario 1. Where it needs 3, 7 and 13 failures for the cell surface temperature, T_{cell}, to rise to 100, 150 and 200 °C, respectively. Also, the figure shows that the cell surface was heated to 100 ° C in a short time within about 35 seconds due to this direct impinging heating by the vent gas jet which represents a serious safety issue. While thermal runaway (T_{cell} = 200°C) starts after about 3 minutes which is shorter than typical single cell experiments such as in Ref. [32], due to this direct heating by the high-temperature vent gas.

To complete the picture, the stairs-like shape curve in Fig. 7(a) is due to the time between sequential failures where there is 4 s time gap, $t_{pre-heating}$, between each two failures

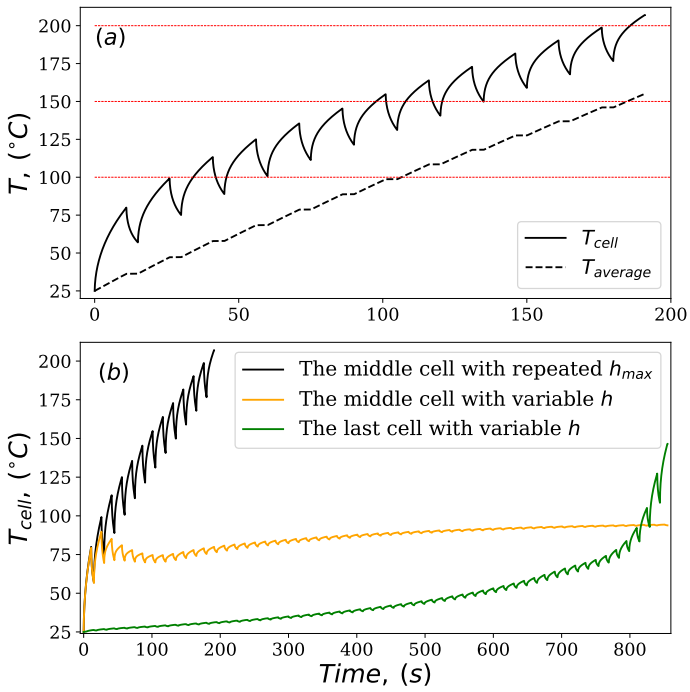

FIGURE 7: (a) cell surface temperature (T_{cell}) and average cell temperature ($T_{average}$) evolution over time for case v7H1 with jet temperature (T_{Jet}) of 800 ∘C (Scenario 1). The red horizontal lines show the three temperatures: 100, 150, and 200 °C, respectively. (b) T_{cell} evolution over time for case v7H1 (Scenario 1), and the avenge variable convection coefficient (h) applied on the middle and last cells.

TABLE 3: Results of LIM1TR simulations for the number of cell failures needed to initiate thermal runaway ($n_{cell,TR}$) in exposed cell to the vent jet, and heat its surface to 100 °C ($n_{cell,100}$) and 150 °C ($n_{cell,150}$). Constant h_{max} of case v7H1 (122.1 W/m^{2}K) and case v5H2 (77.4 W/m^{2}K), and two values of T_{Jet} are used as convective boundary conditions.

Scenario	h_{max} (W/m^{2}K)	T_{Jet} (°C)	$n_{cell,100}$	$n_{cell,150}$	$n_{cell,TR}$
1	122.1	800	3	7	13
2	122.1	500	7	16	27
3	77.4	800	5	11	17
4	77.4	500	10	21	34

where the cell heating slows down due the lack of forced flow from venting in the gap. Emphasizing that there is still conduction to the cell body as it is shown by $T_{average}$ curve, since $T_{average}$ is less than T_{cell}.

After investigating such cases of constant heating by the maximum estimated convection coefficients, we are studying the effect of the distribution of these coefficients along the channel.

3.4.2 Direct Spatially Distributed Heating. As shown in Fig. 5(b), h changes along the module gap as vent gas jet spreads in the channel away from the impingement point. In this part, the effect of the spatial distribution of h on thermal runaway was studied using LIM1TR. Convective boundary conditions of varied h values and constant jet temperature of 800 °C were applied on the cell bottom surface (see Fig. 6). h values used in the simulations are averaged over the cell thickness at the locations along the channel for case v7H1. This section focuses on the heat transfer to the middle cell and last cell in the upper module as thermal runaway propagates along the lower module as shown in Fig. 8.

Figure. 8(a) shows how h, as a function of distance from the failing cell from CFD, is applied to the upper module at two different times. Propagation in the lower module is simplified for this analysis by assuming thermal runaway begins at the middle cell and moves in one direction (to the right) with the same prescribed vent and pre-heating times as Section 3.4.2. This figure shows that as the thermal runaway propagates from cell to cell in the lower module, the middle and last cells in upper module experience different h. Sequentially applying this moving heat flux profile results in heat transfer coefficient vs time resembling the step-shaped depictions shown in Figs. 8(b) and (c). Where in Fig. 8(b), for example, the middle cell is subjected to a jet of temperature of 800 °C and the maximum averaged h for the first venting for 11 s (this represents the vent of the middle cell in Fig. 8(a) at t_1), then 4 s of pre-heating where the temperature of 150 °C and the minimum averaged h are applied on that bottom surface. For the second venting which represents the thermal runaway in the next cell at t_2 in Fig. 8(a), the second maximum averaged h is applied with the 800 °C temperature, then the 4 s of pre-heating of 150 °C temperature and the minimum averaged h are applied; this continues until the last cell goes into thermal runaway in the module. This scenario is flipped for the last cell as shown in Fig. 8(c).

The effect of this distribution in h on the cell surface temperature is shown in Fig. 7(b) for the middle and last cells, and compared with the first scenario of constant h_{max} in Table 3. The results show that there is a significant difference in T_{cell} where it reaches 100 °C fast (less number of failures) for constant h_{max} case compered with the last cell with spatially distributed h. Where, also, the maximum value of T_{cell} for the middle cell with variable h does not reach 100 °C (about 94 °C) as shown in Fig. 7(b). Figure 7(b) shows that cells at different locations in the module are affected differently, where T_{cell} of the last cell ultimately increases more than the middle cell due to gradually heating from channel flow as the propagation front approaches the end of the module; the last cell surface temperature is more than 50 °C higher than the middle cell.

In summary, the study is an attempt to investigate the role of vent gas on thermal runaway propagation, particularly module-to-module propagation, by pure convection. Venting velocity, module gap height, venting temperature, venting time, pre-heating time between two consecutive failures, and other parameters such as varying convection coefficient were considered in this effort. The cells under interest were the middle and last in the upper module assuming direct heating by the gas jet to the bottom surfaces of these cells.

4. CONCLUSION

This work aims to assess the potential safety hazards associated with Li-ion batteries vent gas due to convection in ESSs, and test the ability of these gases to drive the cell directly exposed to them into thermal runaway. It also tries to study the role of vent gas in module-to-module propagation by pure convection. This was achieved by estimating the heat fluxes and convection heat transfer coefficients of the vent gas jet for four cases of two venting velocities and two gap heights between the cells and walls of their module. After that, a thermal runaway model, LIM1TR, was used to impose these convection coefficients on the surface of the target cell to test the possibility of thermal runaway initiation.

The results from the simulated cases show that it requires multiple consecutive cell failures to initiate a thermal runaway in the cell exposed to the vent gas jet due to direct impinging heating where thermal runaway was assumed to occur when cell surface temperature reaches 200 °C. The number of these needed failures to raise the exposed cell surface temperature to a dangerous level is strongly related to vent gas jet temperature and less sensitive to jet convection coefficient where 37.5% decrease in jet temperature has a minimum effect of 90.9% on the number of cell failures, while 36.6% decrease in convection coefficient has a maximum change in the number of failures by 66.7%.

This work shows that the primary role of vent gas in module-to-module propagation could be pre-heating in adjacent modules.

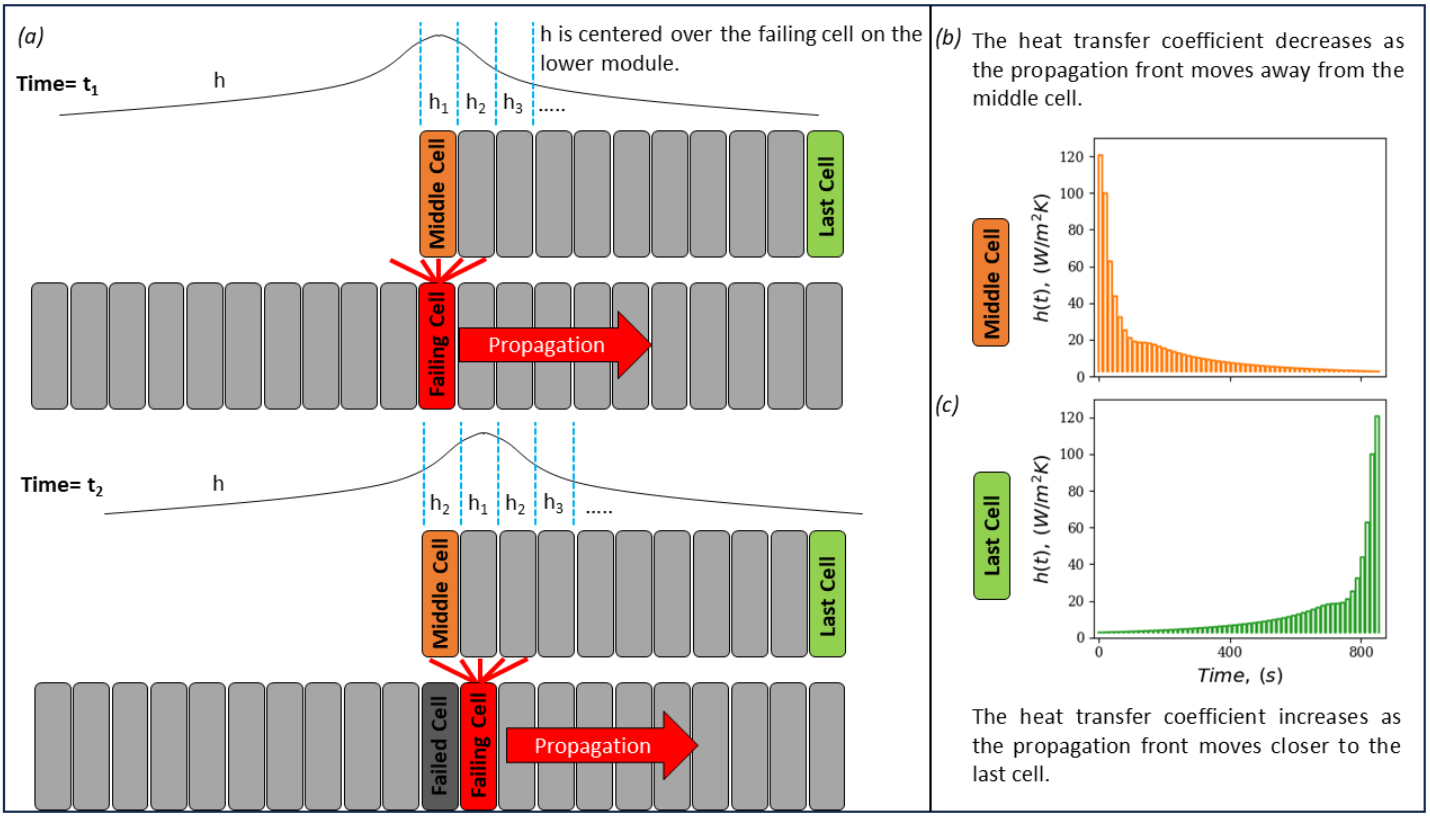

FIGURE 8: (a) Thermal runaway propagation of case v7H1 along right half of the module showing the convection coefficient (*h*) applied on the middle and last cells changes as propagation moves to the right. (b) and (c) the decrease and increase of *h* applied on the middle cell and last cell over time. respectively.

It also shows that the amount of pre-heating of the cells in adjacent modules is spatially dependent on the movement of the propagation front in the failing module.

ACKNOWLEDGEMENTS

This article has been authored by an employee of National Technology & Engineering Solutions of Sandia, LLC under Contract No. DE-NA0003525 with the U.S. Department of Energy (DOE). The employee owns all right, title and interest in and to the article and is solely responsible for its contents. The United States Government retains and the publisher, by accepting the article for publication, acknowledges that the United States Government retains a non-exclusive, paid-up, irrevocable, world-wide license to publish or reproduce the published form of this article or allow others to do so, for United States Government purposes. The DOE will provide public access to these results of federally sponsored research in accordance with the DOE Public Access Plan https://www.energy.gov/downloads/doe-public-access-plan. This paper describes objective technical results and analysis. Any subjective views or opinions that might be expressed in the paper do not necessarily represent the views of the U.S. Department of Energy or the United States Government. This material is based upon work supported by the U.S. Department of Energy, Office of Electricity (OE), Energy Storage Division. SAND2024-XXXX.

REFERENCES

[1] Kim, D. K., Yoneoka, S., Banatwala, A. Z., Kim, Y.-T., and Nam, K., 2018. "Handbook on battery energy storage system". *Asian Development Bank: Manila, Philippines*. URL https://www.adb.org/publications/battery-energy-storage-system-handbook.

[2] EIA, U., 2020. "Battery storage in the united states: an update on market trends". *US Energy Information Administration (EIA)*.

[3] Diaz, L. B., He, X., Hu, Z., Restuccia, F., Marinescu, M., Barreras, J. V., Patel, Y., Offer, G., and Rein, G., 2020. "Meta-review of fire safety of lithium-ion batteries: Industry challenges and research contributions". *Journal of The Electrochemical Society,* ***167***(9), p. 090559.

[4] Ouyang, D., Chen, M., Huang, Q., Weng, J., Wang, Z., and Wang, J., 2019. "A review on the thermal hazards of the lithium-ion battery and the corresponding countermeasures". *Applied Sciences,* ***9***(12), p. 2483.

[5] Feng, X., Ouyang, M., Liu, X., Lu, L., Xia, Y., and He, X., 2018. "Thermal runaway mechanism of lithium ion battery for electric vehicles: A review". *Energy Storage Materials,* ***10***, pp. 246–267.

[6] Baird, A. R., Archibald, E. J., Marr, K. C., and Ezekoye, O. A., 2020. "Explosion hazards from lithium-ion battery vent gas". *Journal of Power Sources,* ***446***, p. 227257.

[7] Said, A. O., Lee, C., Stoliarov, S. I., and Marshall, A. W., 2019. "Comprehensive analysis of dynamics and hazards associated with cascading failure in 18650 lithium ion cell arrays". *Applied Energy,* ***248***, pp. 415–428.

[8] Golubkov, A. W., Fuchs, D., Wagner, J., Wiltsche, H., Stangl, C., Fauler, G., Voitic, G., Thaler, A., and Hacker, V., 2014. "Thermal-runaway experiments on consumer li-ion batteries with metal-oxide and olivin-type cathodes". *Rsc Advances,* ***4***(7), pp. 3633–3642.

[9] Koch, S., Fill, A., and Birke, K. P., 2018. "Comprehensive gas analysis on large scale automotive lithium-ion cells in thermal runaway". *Journal of Power Sources,* ***398***, pp. 106–112.

[10] Essl, C., Golubkov, A., and Fuchs, A., 2020. "Comparing different thermal runaway triggers for two automotive lithium-ion battery cell types". *Journal of the Electrochemical Society,* ***167***(13), p. 130542.

[11] Dispute erupts over what sparked an explosive li-ion energy storage accident. URL https://spectrum.ieee.org/dispute-erupts-over-what-sparked-an-explosive-liion-energy-storage-accident.

[12] Fires raise concern over energy storage battery safety in south korea. URL https://www.infolink-group.com/en/storage/energy-storage-market-trends/fires-raise-concern-over-energy-storage-battery-safety-in-south-korea.

[13] Battery modules "overheat" at vistra's moss landing energy storage facility. URL https://kion546.com/news/local-news/top-stories/2021/09/06/battery-modules-overheat-at-vistras-moss-landing-energy-storage-facility/.

[14] Lamb, J., Orendorff, C. J., Steele, L. A. M., and Spangler, S. W., 2015. "Failure propagation in multi-cell lithium ion batteries". *Journal of Power Sources,* ***283***, pp. 517–523.

[15] Torres-Castro, L., Kurzawski, A., Hewson, J., and Lamb, J., 2020. "Passive mitigation of cascading propagation in multi-cell lithium ion batteries". *Journal of The Electrochemical Society,* ***167***(9), p. 090515.

[16] Feng, X., He, X., Ouyang, M., Lu, L., Wu, P., Kulp, C., and Prasser, S., 2015. "Thermal runaway propagation model for designing a safer battery pack with 25 ah linixcoymnzo2 large format lithium ion battery". *Applied energy,* ***154***, pp. 74–91.

[17] Feng, X., Lu, L., Ouyang, M., Li, J., and He, X., 2016. "A 3d thermal runaway propagation model for a large format lithium ion battery module". *Energy,* ***115***, pp. 194–208.

[18] Li, Q., Yang, C., Santhanagopalan, S., Smith, K., Lamb, J., Steele, L. A., and Torres-Castro, L., 2019. "Numerical investigation of thermal runaway mitigation through a passive thermal management system". *Journal of Power Sources,* ***429***, pp. 80–88.

[19] Kim, J., Mallarapu, A., Finegan, D. P., and Santhanagopalan, S., 2021. "Modeling cell venting and gas-phase reactions in 18650 lithium ion batteries during thermal runaway". *Journal of Power Sources,* ***489***, p. 229496.

[20] A.1 standard solvers. URL https://www.openfoam.com/documentation/user-guide/a-reference/a.1-standard-solvers.

[21] Buoyantpimplefoam solver. URL https://www.openfoam.com/documentation/guides/latest/doc/guide-applications-solvers-heat-transfer-buoyantPimpleFoam.html.

[22] Menter, F., 1993. "Zonal two equation kw turbulence models for aerodynamic flows". In 23rd fluid dynamics, plasmadynamics, and lasers conference, p. 2906.

[23] Menter, F. R., 1994. "Two-equation eddy-viscosity turbulence models for engineering applications". *AIAA journal,* ***32***(8), pp. 1598–1605.

[24] Energy equation in openfoam. URL `https://doc.cfd.direct/openfoam/energy-equation/`.

[25] Barestrand, H., Ljung, A.-L., Summers, J., and Lundström, S., 2023. "Modeling convective heat transfer of air in a data center using openfoam: Evaluation of the boussinesq buoyancy approximation". *OpenFOAM® Journal-V3. 4-Closed,* ***3***, pp. 146–158.

[26] Jaramillo, J. E., Perez-Segarra, C.-D., Rodriguez, I., and Oliva, A., 2008. "Numerical study of plane and round impinging jets using rans models". *Numerical Heat Transfer, Part B: Fundamentals,* ***54***(3), pp. 213–237.

[27] Kennedy, R. W., Marr, K. C., and Ezekoye, O. A., 2021. "Gas release rates and properties from lithium cobalt oxide lithium ion battery arrays". *Journal of Power Sources,* ***487***, p. 229388.

[28] Jaramillo, J., Trias, F. X., Gorobets, A., Pérez-Segarra, C., and Oliva, A., 2012. "Dns and rans modelling of a turbulent plane impinging jet". *International Journal of Heat and Mass Transfer,* ***55***(4), pp. 789–801.

[29] Kurzawski, A., and Shurtz, R., 2019. LIM1TR: Lithium-ion Modeling with 1-D Thermal Runaway v1.0. Tech. Rep. SAND2021-12281, Sandia National Lab, (SNL-NM), Albuquerque, NM (United States).

[30] Armstrong, E., Hansen, M., McConnell, J., and USDOE, 2020. Spitfire, version 1.0, 2.

[31] Hansen, M. A., Hewson, J. C., Armstrong, E., McConnell, J. T., Sutherland, J. C., and Knaus, R. C., 2022. Spitfire v1.02.01.

[32] Archibald, E., Kennedy, R., Marr, K., Jeevarajan, J., and Ezekoye, O., 2020. "Characterization of thermally induced runaway in pouch cells for propagation". *Fire technology,* ***56***(6), pp. 2467–2490.

[33] Kurzawski, A., Gray, L., Torres-Castro, L., and Hewson, J., 2023. "An investigation into the effects of state of charge and heating rate on propagating thermal runaway in li-ion batteries with experiments and simulations". *Fire Safety Journal,* ***140***, p. 103885.